Far-Infrared−Ultraviolet Dielectric Function, Lattice Vibration, and Photoluminescence Properties of Diluted Magnetic Semiconductor $Sn_{1-x}Mn_xO_2$/*c*-Sapphire Nanocrystalline Films

W. L. Yu,[†] W. W. Li,[†] J. D. Wu,[‡] J. Sun,[‡] J. J. Zhu,[†] M. Zhu,[§] Z. G. Hu,*[,†] and J. H. Chu[†]

Key Laboratory of Polar Materials and Devices, Ministry of Education, Department of Electronic Engineering, East China Normal University, Shanghai 200241, People's Republic of China, Key Laboratory for Advanced Photonic Materials and Devices, Ministry of Education, Department of Optical Science and Engineering, Fudan University, Shanghai 200433, People's Republic of China, and Department of Physics, Shanghai Jiao Tong University, Shanghai 200240, People's Republic of China

Received: February 12, 2010; Revised Manuscript Received: April 1, 2010

Optical properties of $Sn_{1-x}Mn_xO_2$ (x from 0.0 to 0.15) nanocrystalline films grown on *c*-plane sapphire substrates have been investigated at room temperature by ultraviolet-infrared transmittance, far-infrared reflectance, and photoluminescence spectra. The X-ray diffraction analysis indicate that the films are of tetragonal rutile structure except for 5% Mn doping, in which the slight orthorhombic phase appears due to the presence of defects and strain. The dielectric functions are successfully determined from 0.025 to 6.5 eV using the Adachi and Lorentz multioscillator dispersion models in the high and low photon energy regions, respectively. The fundamental absorption edge is found to shift toward a lower energy side with increasing Mn composition. The refractive index of pure SnO_2 film is estimated to be the lowest among the $Sn_{1-x}Mn_xO_2$ system. On the other hand, the low E_u transverse optical (TO) phonon frequencies slightly increase with the Mn composition. However, the highest E_u(TO) and A_{2u}(TO) vibration modes present an opposite change trend. Compared with SnO_2 single crystal, four corresponding longitudinal optical (LO) phonon frequencies decrease for the films owing to the variation of the lattice constants and destruction of the crystal symmetry. Photoluminescence spectra of doped SnO_2 films show the remarkable intensity changes and a blue-shift trend compared to pure SnO_2 film. Moreover, a novel emission peak of about 1.56 eV associated with the Mn dopant can be observed. It can be concluded that the Mn incorporation effects are the main contributions because the replacement of Sn with Mn ion can induce the 2p−3d hybridization and result in the electronic band structure modification of the $Sn_{1-x}Mn_xO_2$ films.

I. Introduction

Tin dioxide (SnO_2) is an n-type semiconductor with a wide band gap E_g (about 3.6 eV) at room temperature (RT) and well-known for its applications in gas sensors, transparent conducting electrodes, dye-based solar cells, catalysts, etc.[1–3] With the promising applications in the field of spin electronics for diluted magnetic semiconductors (DMS), transition metal (TM) doped SnO_2 materials have attracted considerable attention due to the theoretical prediction of high Curie temperature and experimental observations of RT ferromagnetism. Recently, Punnoose et al. have shown that Fe doped SnO_2 produced a ferromagnetism with a Curie temperature as high as 850 K; it has been argued that the ferromagnetism is related to the incorporation of Fe into the crystal lattice.[4] Kimura et al. investigated Mn doped SnO_2 films prepared by pulsed laser deposition (PLD) and found that the magnetic moments per Mn site decrease with increasing Mn composition.[5] Xiao et al. also reported remarkable ferromagnetism for Mn doped SnO_2 films at RT, and the coercivity increases with increasing Mn content.[6] Therefore, these results indicate that SnO_2 could be one of the suitable host compounds for DMS realization. No doubt, it is important to study TM doped oxide materials with a wide composition region, in which cations are replaced by TM with different radius and/or charge.[7] Unfortunately, no more studies on the optical properties of TM doped SnO_2 films in a wider photon energy region, especially for optical functions and TM doping effects, have been presented up to now. The optical functions play an important role in the optoelectronic device design. For example, energy transport by exciton and performance of luminescent devices depend on the optical function of the concerned material.[8] Furthermore, the dielectric function, which can be related to the electronic band structure of materials, not only provides basic optical properties but is also critical for developing the novel spin electronics devices.

On the other hand, there are few reports on the lattice vibrations of SnO_2 films, especially in the far-infrared (FIR) region. Hirata et al. described IR reflectance spectra consisting of the IR active E_u and A_{2u} modes between 50 and 900 cm^{-1}.[7] Both Fe and Co doping effects on the structural properties of SnO_2 were obtained using IR and Raman spectroscopic techniques.[9,10] However, no attempt has been made to extract dispersion parameters such as the dielectric function, the frequency of the IR active modes, the oscillator strength, and the damping factor. It is essential to know how the lattice parameters of $Sn_{1-x}Mn_xO_2$ (SMO) films change as a function of Mn composition, in order to understand the composition effects on the vibration properties of the SMO films. Of course, the phonon mode assignation is necessary to further study the

* Corresponding author. E-mail: zghu@ee.ecnu.edu.cn.
[†] East China Normal University.
[‡] Fudan University.
[§] Shanghai Jiao Tong University.

10.1021/jp101344d
Published on Web 04/14/2010

coupling between the phonon and magnon in the DMS system. Moreover, photoluminescence (PL) properties of SnO_2 play an important role in improving optoelectronic device performance. The PL spectrum can be employed to study the structure or defect states of films, which serves as a technique to identify additional defect levels generated by additive incorporation. Note that most PL properties have been presented mainly from SnO_2 nanostructures. It is widely accepted that PL emission bands of SnO_2 films and nanostructures are derived from oxygen vacancy centers or surface states (e.g., tin vacancies/interstitials).[11−14] Recently, Yuan et al. observed a red band at about 590 nm in the SnO_2/*p*-Si heterojunction. It was argued that the electrons in the conduction band first relax nonradiatively to the defect states and then radiatively recombine with the holes in the valence band.[15] However, few reports on the PL spectra from TM doped SnO_2 materials have been given. It was reported that PL spectra of Fe doped SnO_2 films show an obvious change in emission intensity and blue-shift trend with the magnetic dopant.[16] Nevertheless, the PL properties from TM doped SnO_2 layers are still scarce and need further investigations to clarify the magnetic element energy levels in the electronic band structure.

The focus of the present work is to study the optical functions, IR active phonon modes, and PL emission bands of diluted magnetic SMO films on *c*-plane sapphire substrates in the far-infrared−ultraviolet photon energy range. The theoretical models are applied to reproduce the experimental transmittance and reflectance spectra well. The effects from the Mn doping on the optical properties have been discussed in detail.

II. Experimental Details

Film Preparations. Nanocrystalline SMO films were deposited by PLD in the present work. The SMO targets in the diameter of 3 cm were prepared using a conventional solid-state reaction sintering. During the preparation, MnO powder was mixed with SnO_2 powder (99.99%) in which the Mn mole fraction was varied as 2.5, 5, 7.5, 10, 12.5, and 15%, respectively. Double-side polished *c*-sapphire wafers were used as the substrates. The substrates were rigorously cleaned in pure ethanol with an ultrasonic bath and were rinsed several times by deionized water before the deposition. The growth chamber was first pumped down to a base pressure of 10^{-4} Pa. A pulsed Nd:YAG (yttrium aluminum garnet) laser (532 nm wavelength, 5 ns duration), which working at a repetition rate of 10 Hz and an energy of 40 mJ/pulse, was used for target ablation. The films were grown immediately after the target was preablated. The distance between the target and substrate was kept at 3 cm, and the deposition time was set to about 30 min. Then, the films were annealed at 1000 °C in air atmosphere by a rapid thermal annealing process. A detailed preparation of the films can be found in refs 17 and 18.

XRD and Optical Characterizations. The crystalline structures of the SMO films on *c*-sapphire substrates were analyzed by X-ray diffraction (XRD) using Cu Kα radiation (D/MAX-2550 V, Rigaku Co). The optical transmittance experiments were done with a double beam ultraviolet−near-infrared (UV−NIR) spectrophotometer (PerkinElmer Lambda 950) from 190 to 3300 nm (0.38−6.5 eV) with a spectral resolution of 2 nm. Because the sapphire substrate is not transparent in the FIR region, the near-normal incident (∼10°) IR reflectance measurements were performed over the frequency range from 200 to 2000 cm^{-1} (0.025−0.25 eV) using a Fourier transform infrared spectrometer (Bruker Vertex 80 V). The spectral resolution was 2 cm^{-1} in the low frequency and 4 cm^{-1} in the high frequency, respectively. The different beamsplitters, optimized KBr or 6-μm-thick Mylar, were used with DTGS detectors for each IR region. Gold and aluminum mirrors, whose absolute reflectances were measured, were taken as the references for the spectra in the high and low frequency regions, respectively. Note that there is no obvious dispersion variation in the energy gap 0.25−0.38 eV due to the transparency of the SMO materials. Therefore, the dielectric function can be smoothly connected in the experimental gap. PL spectra were recorded by a Jobin-Yvon LabRAM HR 800 UV spectrometer with a He−Cd laser as the excited light, which is operated at a wavelength of 325 nm (3.82 eV). The samples were at RT for all measurements, and no mathematical smoothing has been performed for the experimental data.

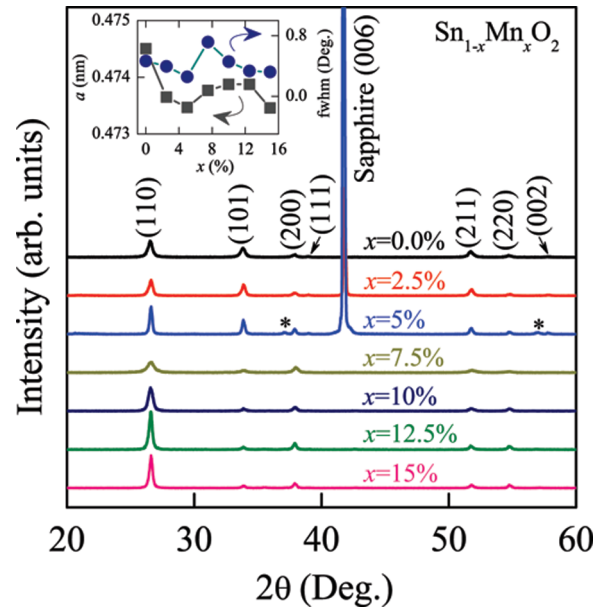

Figure 1. XRD patterns of the $Sn_{1-x}Mn_xO_2$ films on *c*-sapphire substrates at different Mn compositions. Note that the (006) diffraction peak from the sapphire is cut because of the much stronger intensity. The inset shows various values of full width at half-maximum and *a*-axis lattice constant evaluated from the peak (110). The symbol ∗ indicates the observed trace of the orthorhombic phase.

III. Results and Discussion

Structural Analysis. Figure 1 shows the diffraction peaks (110), (101), (200), (211), and (220), etc., indicating that the films are polycrystalline materials with good crystallization. It should be emphasized that the (006) diffraction peak from the sapphire substrate can be observed in the SMO films doped with 2.5 and 5% Mn. It generally reveals the SMO films have the tetragonal rutile structures. Nevertheless, the diffraction pattern of the film doped with 5% Mn displays two additional weak peaks (labeled by ∗), which are derived from the orthorhombic phase owing to the presence of defects and strain.[19] Note that the (101) diffraction peak becomes much weaker and the (110) diffraction peak becomes stronger for the films with $x \geq 7.5\%$, which may be ascribed to the Mn doping contributions. It indicates that the lower and higher Mn compositions could result in the different crystalline formation. The full width at half-maximum (fwhm) and *a*-axis lattice constant calculated from the (110) diffraction peak can be seen in the inset of Figure 1. The average value of the *a*-axis lattice constant is estimated to be about 4.738 Å, which is slightly larger than those reported in Mn doped SnO_2 films prepared by sol−gel and spray

pyrolysis methods.[6,20] This discrepancy can be ascribed to different lattice mismatch, stress, and/or strain, which can be normally affected by the deposition technique, substrate material, and film thickness. Correspondingly, the fwhm and lattice constant present different variation trends for the lower and higher Mn compositions. From Figure 1, the fwhm is initially decreased with the doping composition and increased to the maximum with the 7.5% Mn concentration. An obvious increment of both structure parameters for the SMO film with $x = 7.5\%$ indicates a significantly different doping mechanism.[9,19] On the other hand, it can be found that the SMO films are nanocrystalline with an average grain size of about 24 nm according to Scherrer's equation. The minimum grain size belongs to the sample with $x = 7.5\%$, which is also similar to the result from different preparation methods.[20] It was reported that the undoped SMO grains are spherical; however, with increased doping concentration, the grains can be changed from spherical to elongated ones along the *a*-axis.[19,21] Moreover, there is a limiting dopant composition, which has a strong relation to the structural changes.[19] Therefore, it can be concluded that the Mn incorporation causes the reduction of lattice space symmetry and crystal distortion in the film structure, and then further affects the optical properties of the SMO material.

Theoretical Consideration. A three-phase layered structure (air/film/substrate) was used to calculate the UV−NIR transmittance and FIR reflectance spectra of the SMO films.[22,23] The optical component of each layer is expressed by a 2×2 matrix. Suppose the dielectric function of the film is $\tilde{\varepsilon}$, the vacuum is unity, and the substrate is $\tilde{\varepsilon}_s$. The resultant matrix M_r is described by the following product form

$$M_r = M_{vf} M_f M_{fs} \tag{1}$$

Here, the interface matrix between the vacuum and film has the form

$$M_{vf} = \frac{1}{2\sqrt{\tilde{\varepsilon}}} \begin{bmatrix} (\sqrt{\tilde{\varepsilon}} + 1) & (\sqrt{\tilde{\varepsilon}} - 1) \\ (\sqrt{\tilde{\varepsilon}} - 1) & (\sqrt{\tilde{\varepsilon}} + 1) \end{bmatrix} \tag{2}$$

and the propagation matrix for the film with thickness is described by the equation

$$M_f = \begin{bmatrix} \exp(i2\pi\sqrt{\tilde{\varepsilon}} d/\lambda) & 0 \\ 0 & \exp(-i2\pi\sqrt{\tilde{\varepsilon}} d/\lambda) \end{bmatrix} \tag{3}$$

where λ is the incident wavelength, and correspondingly the interface matrix between film and substrate is

$$M_{fs} = \frac{1}{2\sqrt{\tilde{\varepsilon}_s}} \begin{bmatrix} (\sqrt{\tilde{\varepsilon}_s} + \sqrt{\tilde{\varepsilon}}) & (\sqrt{\tilde{\varepsilon}_s} - \sqrt{\tilde{\varepsilon}}) \\ (\sqrt{\tilde{\varepsilon}_s} - \sqrt{\tilde{\varepsilon}}) & (\sqrt{\tilde{\varepsilon}_s} + \sqrt{\tilde{\varepsilon}}) \end{bmatrix} \tag{4}$$

Thus, the transmittance T and reflectance R can be readily obtained from

$$T = \mathrm{Real}(\sqrt{\tilde{\varepsilon}}) \left| \frac{1}{M_{r1,1}} \right|^2, \qquad R = \left| \frac{M_{r1,0}}{M_{r1,1}} \right|^2 \tag{5}$$

The multireflections from the substrate are not considered in eq 5. It should be emphasized that the absorption from the substrate must be taken into account to calculate the transmittance of the film−substrate system.

As we know, the reliability of the fitting method mainly depends on the validity of the dielectric function model. For wide band gap semiconductor materials, the dielectric response, which can be described by the contribution from the lowest three-dimensional M_0 type critical point (CP), is written as the following Adachi model:

$$\tilde{\varepsilon}(E) = 1 + \frac{A_0[2 - (1 + \chi_0)^{1/2} - (1 - \chi_0)^{1/2}]}{E_g^{3/2} \chi_0^{\ 2}} \tag{6}$$

Here, $\chi_0 = (E + i\Gamma)/E_g$, E_g is the fundamental optical transition energy, E is the incident photon energy, and A_0 and Γ are the strength and broadening parameters of the E_g transition, respectively. The above Adachi model is successfully applied in many semiconductor and dielectric materials.[24,25] On the other hand, the IR dielectric response function can be expressed by the Lorentz multioscillator model for the optical phonons. The dielectric functions of the SMO films can be written as

$$\tilde{\varepsilon}(\omega) = \varepsilon_\infty + \sum_{k=1}^{4} \frac{S_k \omega_{TO,k}^{\ 2}}{\omega_{TO,k}^{\ 2} - \omega^2 - i\omega\Gamma_k} \tag{7}$$

Here, ε_∞, S_k, $\omega_{TO,k}$, Γ_k, and ω represent, in order, the high frequency dielectric constant, TO phonon strength, TO phonon frequency, damping parameter of the TO phonon, and frequency of the incident light, respectively.[22] The free carrier effects are neglected because the SMO films are nominally undoped. Note that it is nearly impossible that the Adachi or Lorentz model can explain the complicated optical response behavior of semiconductors and insulators in the wider photon energy region. Therefore, different function models corresponding to the interband/intraband electronic transition mechanism are necessary.[26] The dielectric functions of the SMO films can be uniquely determined by fitting the function model to the experimental data from the FIR to UV photon energy regions.

It should be emphasized that the present SMO films have polycrystalline formation, as indicated by the XRD patterns. The grain size and boundary may affect the optical response due to the scattering behavior and average anisotropic effect. In addition, there is generally the surface rough layer for the PLD derived SMO films.[25−27] The porous surface layer could be several nanometers, which is much less than the film thickness of about several hundred nanometers. Fortunately, the surface rough layer can be neglected owing to a smaller thickness value, whose contribution should be slight in the evaluation of the optical properties. The relatively big light spot (about 4 mm in diameter) and normal-incident configuration, which cannot be sensitive to grain size/boundary and void density, are used in the present transmittance and reflectance experiments. In particular, grain and void contribution effects could be tiny for the infrared reflectance spectra due to the longer infrared wavelength, whose value is much larger than the grain size and void dimension. In addition, from the optical constants discussed later, one can also conclude that the SMO films are dense enough for the optical analysis, as compared with the reported values. Therefore, the three-phase layered structure and the Adachi dielectric model can be reasonably acceptable for the present SMO films.

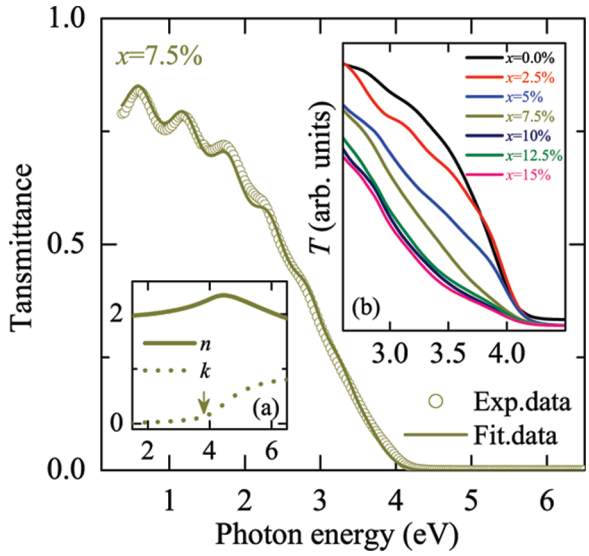

Figure 2. Experimental and best-fit transmittance spectra of the film doped with 7.5% Mn from the UV to NIR photon energy region. (a) The optical functions of the film doped with $x = 7.5\%$ obtained by the Adachi model. (b) An enlarged region of 2.5−4.5 eV for the $Sn_{1-x}Mn_xO_2$ films from the transmittance spectra.

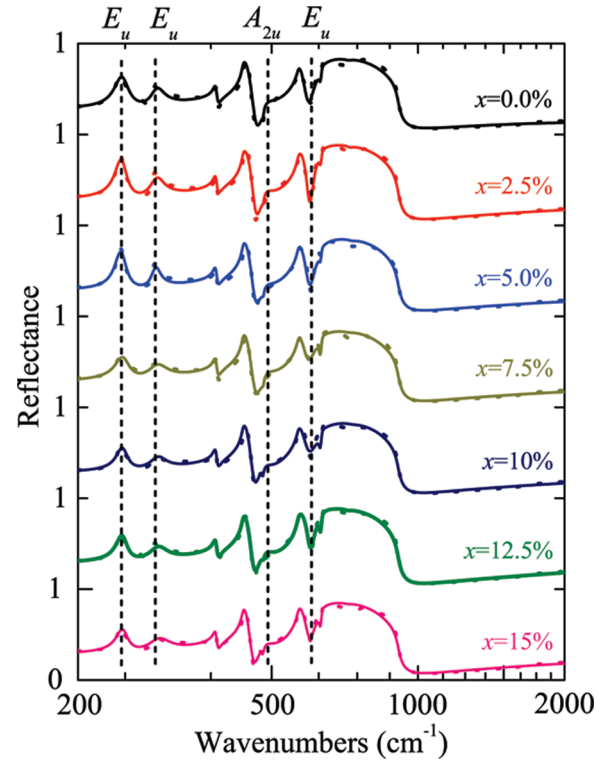

Figure 3. Experimental IR reflectance spectra (dotted lines) and the best-fit results (solid lines) of the $Sn_{1-x}Mn_xO_2$ films. Each spectrum is successively shifted by 1.0 in the vertical direction. The horizontal coordinate is the logarithmic unit to enlarge the lattice vibration region. The dashed lines clearly indicate the phonon modes.

UV−NIR Transmittance Characteristics. To understand the electronic structure modification by the Mn composition, the optical transmittances of the SMO films were recorded at RT. As an example, a best-fit spectrum by the Adachi model for the sample doped with 7.5% Mn is shown in Figure 2. The spectral patterns are similar to those reported by Kimura et al.[5] An interference effect (due to the finite thickness of the films) below about 2.5 eV is observed, indicating that the film is transparent in the region. The measured transmittance spectra near the band gap are plotted in inset b of Figure 2. As can be seen, the absorption edge shifts to the lower energy side with increasing Mn composition except for the film with 12.5% Mn. It suggests that matrix incorporation of Mn atoms occurs, which is well-known to happen in DMS materials.[28]

The absorption edge of SnO_2 has been assigned to interband transitions from the valence band edge with O 2p orbitals to the conduction band edge with Sn 5s orbitals.[29] In Mn doped rutile SnO_2, O ions around Mn ions form an octahedral crystal field, splitting 3d orbitals into lower t_{2g} states and upper e_g states.[30] The three 3d (t_{2g}) states are occupied, and the other three t_{2g} and four e_g states are empty and located inside the band gap form by Sn 5s- and O 2p-like bands.[31] Moreover, the filled Mn 3d states are strongly hybridized with the O 2p states, giving a broad band with a width comparable to O 2p states.[30] Therefore, the Mn increasing can affect the O 2p and Mn 3d orbital distributions, which will induce the t_{2g} and e_g states located at different levels in the energy space. This will further result in the absorption edge vibrations in the SMO films. It is pointed out here that the broad in-gap absorption for 2.5−4 eV with some small hump, which is difficult to identify, may be related to hybridization of the SMO films as well.[5] There are also some indications of hybridized transitions in the optical transmittance spectra of Mn doped ZnO.[32,33] Singh et al. reported that the d states of TM ion split under the influence of the crystal field, resulting in the high spin configuration of d electrons and the impurity states undergo hybridization with valence p states of the host compound.[32] The similar phenomena may occur in the present SMO films due to the incorporation of Mn into the SnO_2 host lattice. In addition, all films exhibit a strong absorption beyond the photon energy of about 4.1 eV, whose transmissions are down to zero. The behavior can be derived from the fundamental band gap and high energy critical point transitions, which cannot be detected by the present transmittance spectra.

FIR Reflectance Spectra. Generally, SnO_2 with the rutile structure belongs to the space group D_{4h}^{14}, of which the normal lattice vibration at the Γ point of the Brillouin zone is given as follows on the basis of group theory: $\Gamma = A_{1g}(R) + A_{2g}(F) + A_{2u}(IR) + B_{1g}(R) + B_{2g}(R) + 2B_{1u}(F) + E_g(R) + 3E_u(IR)$.[7,34] Among these vibrations, E_u and A_{2u} modes are IR active; A_{1g}, B_{1g}, B_{2g}, and E_g are Raman active modes; and modes A_{2g} and B_{1u} are optically inactive. For four IR active modes, the expected positions of transverse optical (TO) and longitudinal optical (LO) phonon frequencies from single-crystal SnO_2 are located at $3E_u$ at 244 cm^{-1} (TO), 276 cm^{-1} (LO), 293 cm^{-1} (TO), 366 cm^{-1} (LO), 618 cm^{-1} (TO), and 770 cm^{-1} (LO) and at A_{2u} at 477 cm^{-1} (TO) and 705 cm^{-1} (LO), respectively.[34] IR spectroscopy is a very powerful technique to study the E_u and A_{2u} phonon mode behavior of the SMO films. Figure 3 presents the experimental IR reflectance spectra of the SMO films by the dotted lines. Compared with the highly reflecting sapphire substrate,[35] the peaks from the SMO films are observed in the range 200−2000 cm^{-1} (0.025−0.25 eV). Two peaks located at about 244 and 290 cm^{-1} can be assigned to the low frequencies of E_u (TO) phonon modes. The sharp dip observed nearly at 607 cm^{-1} is also characterized by the E_u (TO) phonon mode. A small band around 480 cm^{-1} is identified from the A_{2u} (TO) mode. In view of these results, it indicates that the $3E_u$ (TO) and A_{2u} (TO) phonon frequencies appear around 200−800 cm^{-1} in the IR reflectance spectra of polycrystalline SMO films, which are close to those found in single crystal SnO_2.[34] Moreover, the IR spectral lineshapes corresponding to different Mn compositions were not changed because the doping composition only

TABLE 1: Parameter Values of the Lorentz Multi-Oscillator Model for the $Sn_{1-x}Mn_xO_2$ Films Determined from the Simulation to Infrared Reflectance Spectra in Figure 3[a]

					E_u			E_u			E_u			A_{2u}	
sample	x (%)	thickness (nm)	ε_∞	S_1	$\omega_{TO,1}$ (cm^{-1})	Γ_1 (cm^{-1})	S_2	$\omega_{TO,2}$ (cm^{-1})	Γ_2 (cm^{-1})	S_3	$\omega_{TO,3}$ (cm^{-1})	Γ_3 (cm^{-1})	S_4	$\omega_{TO,4}$ (cm^{-1})	Γ_4 (cm^{-1})
A	0.0	561	3.74	2.42	246	9.28	1.17	290	15.4	0.90	607	39.2	1.16	481	39.9
		(26)	(0.09)	(0.33)	(1.27)	(2.70)	(0.28)	(2.47)	(6.19)	(0.09)	(1.39)	(2.75)	(0.10)	(2.09)	(5.57)
B	2.5	431	4.51	3.26	245	5.73	1.75	290	16.0	1.04	611	22.9	1.56	480	35.6
		(24)	(0.14)	(0.37)	(0.87)	(1.68)	(0.35)	(2.24)	(5.47)	(0.10)	(1.01)	(1.9)	(0.14)	(1.63)	(4.24)
C	5.0	445	4.35	2.93	245	5.75	1.19	289	9.97	1.15	612	35.5	1.51	478	38.3
		(25)	(0.14)	(0.36)	(0.93)	(1.79)	(0.28)	(1.78)	(4.19)	(0.13)	(1.35)	(2.61)	(0.15)	(1.74)	(5.20)
D	7.5	441	4.46	2.36	247	12.4	1.65	291	23.9	1.02	603	45.8	1.80	479	43.9
		(22)	(0.12)	(0.43)	(1.52)	(3.80)	(0.41)	(3.28)	(9.03)	(0.11)	(1.67)	(3.29)	(0.15)	(1.68)	(5.07)
E	10	406	4.53	2.07	247	9.72	1.42	292	21.3	1.26	607	52.7	1.80	476	35.5
		(24)	(0.15)	(0.40)	(1.41)	(3.34)	(0.40)	(3.54)	(9.53)	(0.14)	(1.90)	(3.25)	(0.16)	(1.36)	(4.15)
F	12.5	352	5.01	2.65	246	8.62	1.94	292	22.9	0.92	609	26.9	2.45	476	37.2
		(22)	(0.19)	(0.41)	(1.08)	(2.47)	(0.43)	(3.05)	(8.10)	(0.10)	(0.99)	(2.36)	(0.21)	(1.21)	(3.44)
G	15	430	4.64	2.06	247	10.1	1.78	294	27.7	0.95	608	37.7	2.08	475	39.0
		(21)	(0.13)	(0.39)	(1.35)	(3.26)	(0.42)	(3.74)	(10.2)	(0.09)	(1.30)	(2.79)	(0.16)	(1.31)	(3.91)

[a] The 90% reliability of the fitting parameters is given in parentheses.

slightly affects the phonon frequency, intensity, and broadening. Since the oblique incidence (~10°), the broad band at 660−780 cm^{-1} in the reststrahlen band of the sapphire is regarded as the E_u (LO) polar mode. The similar phenomenon can also be observed in polycrystalline SnO_2.[7,36] Owing to the lattice distortions, the highest phonon frequency E_u related to the vertical displacements of Sn and O ions is overlapped with the A_{2u} phonon mode, which is ascribed to the parallel relative displacements.[36] The reflectance strength gradually approaches 18% for the films beyond a frequency of 1000 cm^{-1}, which suggests that the films are transparent in the region. The reflectance spectra below 200 cm^{-1} are overlapped with each other for all films and sapphire (not shown), indicating further that the contributions from the free carriers can be negligible.

The calculated spectra with the Lorentz multioscillator model are also shown in Figure 3 with the solid lines. A good agreement between the calculated and experimental data is obtained in the entire frequency region. The best fit parameters of the Lorentz multioscillator model together with the fitting errors are listed in Table 1. The thickness of the film doped with 12.5% Mn (352 nm) is the smallest, as compared to the other films with a thickness between 406 and 561 nm. Nevertheless, the film ($x = 12.5\%$) has a maximum of ε_∞ among the SMO films. It should be noted that the ε_∞ value of the SMO films varies approximately from 3.74 ± 0.09 to 5.01 ± 0.19, which is slightly higher than the reported values ($\varepsilon_{\infty\parallel} = 4.17$, $\varepsilon_{\infty\perp} = 3.78$) of single-crystal SnO_2[37] except for the pure SnO_2 film. In addition, the values of the TO mode strength (S) for the high phonon frequencies E_u and A_{2u} with the Mn compositions are larger than those of pure SnO_2 film. It could be attributed to the structure variations of the SMO films from the Mn introduction and stresses between the film and substrate due to the diverse thickness.

Optical Functions from 0.025 to 6.5 eV. Optical function of DMS materials is an important parameter for optoelectronic and spinelectronic device design. Figure 4 shows the derived refractive index (n) and the extinction coefficient (k) spectra from the Adachi and Lorentz multioscillator models in the different photon energy regions, respectively. The spectral shapes are found to be similar for all films. To clarify, optical functions of the film doped with 7.5% Mn are shown in inset a of Figure 2 for the UV−NIR photon energy region. The dispersion function can be roughly separated into three specific parts: a lattice vibration one (labeled with "I"), a transparent

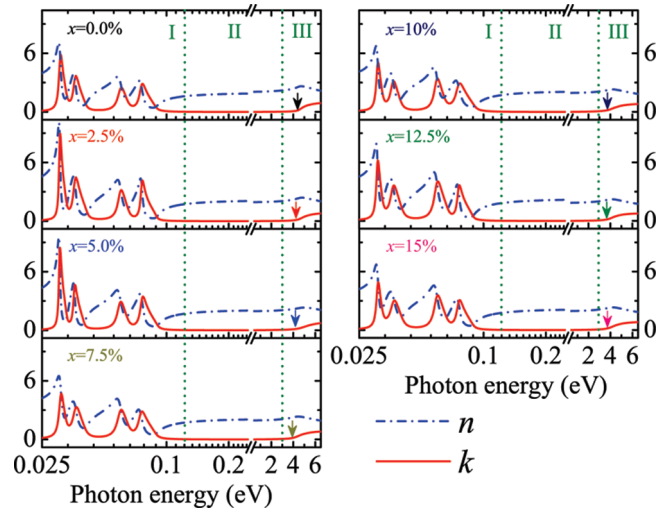

Figure 4. The refractive index n (dash−dotted lines) and extinction coefficient k (solid lines) in the photon energy region of 0.025−6.5 eV for the $Sn_{1-x}Mn_xO_2$ films. The arrows indicate that the absorption edge decreases with increasing Mn composition. To clarify, the horizontal coordinates are the logarithmic units.

oscillating one (labeled with "II"), and an absorption one (labeled with "III") at higher photon energy. In the lattice vibration region, where the dispersion is mainly from infrared optical phonon modes, the intensities of all peaks are found to change, indicating that the Mn incorporation might be responsible for the local disorder. As previously discussed, the Mn doping results in the lattice distortion and reduction in lattice space symmetry. At the limited energy of 0.025 eV (200 cm^{-1}), n of pure SMO film has the lowest value and changes from about 3.98 to 4.6 corresponding to different compositions. The remarkable increment of n indicates the disorder in the lattice introduced by the Mn doping again. On the other hand, k is very small at 0.025 eV, suggesting that it is reasonable to ignore contributions from the free carriers. At about 0.03 eV (245 cm^{-1}), the strongest peak intensities of k varies from 4.8 to 9 with the Mn composition. Interestingly, the intensity abruptly increases for the samples of 2.5 and 5.0% Mn and then falls with the Mn composition further increasing. It is probably related to the crystalline quality of the films, which is also confirmed by the XRD experiments.

In the wide transparent region, both n and k are well connected though different function models are applied. Here,

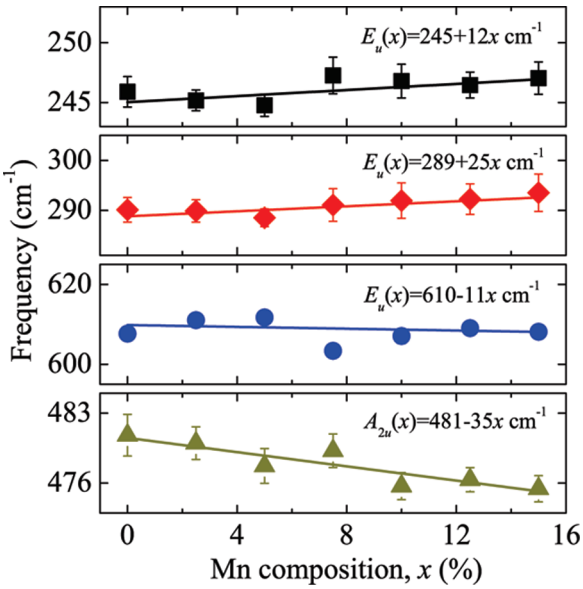

Figure 5. Mn composition dependence of $3E_u$(TO) and A_{2u}(TO) phonon frequencies for the $Sn_{1-x}Mn_xO_2$ films. Note that the solid lines are the linear fitting results to guide the eyes.

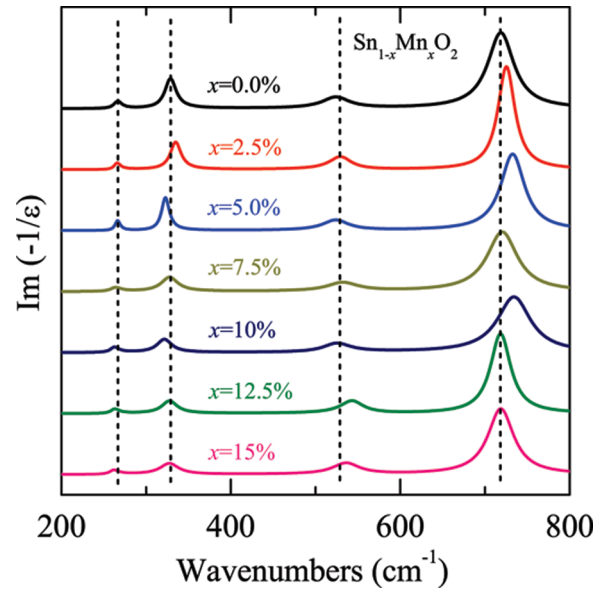

Figure 6. Dielectric loss function Im($-1/\varepsilon$) of the $Sn_{1-x}Mn_xO_2$ films with different Mn compositions. Note that the dashed lines are applied for clarification.

k is down to zero and n is close to a constant. The n values are located between 1.88 and 2.17 with Mn compositions at an energy of 0.25 eV (2000 cm^{-1}). These values are slightly higher than the reported value (about 1.95) obtained from the transmittance spectra of SnO_2 films at a wavelength of 1550 nm.[38] In addition, n increases with the photon energy and approaches the maximum, and then decreases with further increasing photon energy. While k has a sharp feature near 4 eV, slowly increases up to the present measurement limitation (6.5 eV). It suggests that the strong photon absorption appears, showing the interband transition behavior. Note that the onset absorption edge decreases with increasing Mn composition, which can be interpreted by the previously mentioned hybridization for the SMO films. At 6.5 eV, the k value of pure SMO film is larger than those of the others. Such a reduction is explained by increasing scattering because of the crystal lattice disorder.[39]

Lattice Vibrations. A relation between the phonon frequencies and Mn compositions is displayed in Figure 5. The low phonon frequencies of E_u (TO) can be well expressed by (245 + 12x) and (289 + 25x) cm^{-1}, respectively. It suggests that the phonon frequencies slightly increase with the Mn composition. In contrast, the highest phonon modes E_u (TO) and A_{2u} (TO) present a decreasing trend with the Mn composition. A linear dependency on the Mn composition can be described by (610 − 11x) and (481 − 35x) cm^{-1}. It was reported that the E_u mode in the region 615−630 cm^{-1} for Fe doped SnO_2 films from the absorption spectra is assigned to the IR active asymmetric Sn−O stretching mode, whose frequency shifts down as the Fe composition increases. The a-axis lattice parameter linearly decreases as the Fe composition increases from 0.0 to 0.05.[9] Therefore, it is reasonable that Mn has been successfully incorporated into the SnO_2 host lattice. The linear dependency could be due to the variation of the lattice constants in the SMO films. Figure 6 depicts the dielectric loss function Im($-1/\varepsilon$) for the SMO films. As we know, the LO phonon modes correspond to the peaks in Im($-1/\varepsilon$). It should be emphasized that $3E_u$ (LO) and A_{2u} (LO) are observed at about 264, 328, 725, and 529 cm^{-1}, respectively. These values are less than those reported from single crystal SnO_2.[34] It can be ascribed to polycrystalline structure and substrate material, which can affect the phonon mode characteristics of the SMO films. Moreover, the positions

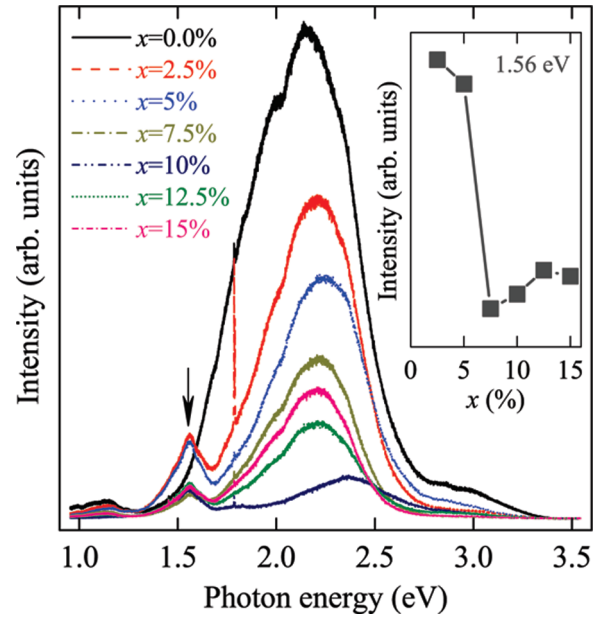

Figure 7. Photoluminescence spectra of the $Sn_{1-x}Mn_xO_2$ films in the photon energy range of 0.9−3.6 eV. The arrow indicates the novel peak position, and the inset shows the corresponding peak intensities change with the Mn compositions at about 1.56 eV.

of the four LO vibrations vary with the Mn composition. The maximal discrepancy of the highest phonon frequency E_u (LO) is about 18 cm^{-1}, as compared with the pure SnO_2 sample. From this viewpoint, it can be concluded that the effect from the Mn introduction plays an important role in the lattice vibration properties. The present work provides crucial information on the IR phonon modes of TM doped SnO_2 films.

Photoluminescence Bands. In order to further understand the Mn effects on the optical properties of the SMO films, PL spectra are presented in Figure 7. There is a distinct difference for the SMO films in the measured energy region. It has been confirmed that the sharp emission peak at about 1.79 eV (694 nm) is related to the sapphire substrate[40] and various thicknesses of films, which can result in the peak intensity variation. There are many reports which show a broad PL band centered in the

range 318−640 nm for SnO_2.[11–14,41–43] However, the high energy band emission, such as 318 nm (3.9 eV) and 350 nm (3.5 eV), is not observed by the present measurement owing to the detection limitation and/or the dipole-forbidden nature of first transition in SnO_2 .[40,44] All spectra exhibit two broad emissions centered at around 2.38−2.15 and 2 eV. The positions of both peaks for the pure SnO_2 sample are very close to those of SnO_2 zigzag nanobelts, which are related to the crystalline defects induced during the growth.[43] Furthermore, the second PL peak is also reported to be caused by a transition between the combined oxygen vacancy defect states, which are located in the band gap of SnO_2 nanostructures.[45] First principle calculation shows that oxygen vacancy and tin interstitial can form easily in SnO_2 material because they have surprisingly low formation energies and strong mutual attractions.[44] Thus, these defects can exist and act as trapped states in the SMO films because the oxygen pressure is fixed during the fabrication. On the other hand, the doping of Mn could provide the influence on the distribution of oxygen vacancy due to the partial replacement of Sn with Mn and Mn filling in the interstitial. When the tin interstitial was affected by the Mn doping, the oxygen vacancy can be correspondingly changed owing to the interaction and further result in the line shape and intensity variations of the above two PL emission bands. In addition, it can be clearly seen that the intensity reductions of both peaks are more drastic until the film doped with 10% Mn. The position of the first peak has an obvious blue-shift with a maximum energy shift of 0.22 eV compared with the pure SnO_2 film. The behavior can be ascribed to the oxygen vacancies and doped Mn ions. The Mn ions can lead to reduction of donor type oxygen vacancies; then, the peak intensity related to oxygen vacancy correspondingly decreases. A similar situation is also reported in Fe doped SnO_2 films.[16]

It should be emphasized that a new peak is observed at about 1.56 eV except for pure SnO_2 film. Therefore, the novel emission peak should be derived from the Mn introduction. The incorporation of Mn in the films is confirmed, and its level is located inside the band gap, forming Sn 5s- and O 2p-like bands.[31] It can be found that the position is kept as a constant, but its intensity is obviously changed. As can be seen in the inset of Figure 7, the intensities for the films doped with 2.5 and 5% Mn are stronger than those of other SMO films. A similar phenomenon is also observed in XRD measurements and optical functions. It again suggests a different doping mechanism for the lower and higher Mn compositions. Note that the particular case also emerges in the sample of $x = 7.5\%$, whose minimum intensity is consistent with its grain size mentioned above. According to the Scherrer equation, the grain size is inversely proportional to the fwhm. On the basis of the effective mass approximation theory,[46] the electronic transition is inversely proportional to the square of the grain size for the low dimensional system, as compared to the bulk material. The PL peaks can be strikingly affected due to different grain sizes, which results in the appearance of the so-called quantum confinement effect in the SMO nanocrystalline films. It reveals that the new peak is attributed to the doped Mn ion and the variation of intensities is a result of different *a*-axis lattice constants and fwhm/grain size. As stated before, the replacement of Sn with Mn ion can affect the 3d−2p hybridization strength and result in the electronic band structure variations of the SMO films. Thus, it can affect the PL properties of the SMO films with different Mn compositions. In order to further clarify the physical behavior, optical experiments at low temperatures are necessary in the future.

IV. Conclusion

The Mn composition dependence of the SMO (x from 0.0 to 0.15) films grown on *c*-plane sapphire substrates by PLD have been determined with the aid of UV−NIR transmittance, FIR reflectance, and PL spectra. The absorption edge has a red-shift with the Mn increasing. The $3E_u$(TO) and A_{2u}(TO) phonon frequencies linearly depend on the Mn composition. The $3E_u$(LO) and A_{2u}(LO) from the dielectric loss functions Im($-1/\varepsilon$) are shifted toward a lower frequency, as compared with the single crystal. Moreover, three PL emission peaks and the blue-shift trend are observed, which are related to oxygen vacancies and the Mn doping effects. In particular, there is a novel PL peak around 1.56 eV except for the pure SnO_2 film. It can be concluded that the 2p−3d hybridization from the replacement of Sn with Mn, which results in the electronic band structure variation, mainly contributes to the experimental phenomena. The results about the SMO films are crucial for potential applications of SnO_2-based optoelectronic and spinelectronic devices.

Acknowledgment. This work was supported by Natural Science Foundation of China (Grant No. 60906046), Major State Basic Research Development Program of China (Grant No. 2007CB924901), Program of New Century Excellent Talents, MOE (Grant No. NCET-08-0192), and Shanghai Municipal Commission of Science and Technology Project (Grant Nos. 08JC1409000, 08520706100, and 09ZZ42).

References and Notes

(1) Selvan, R. K.; Perelshtein, I.; Perkas, N.; Gedanken, A. *J. Phys. Chem. C* **2008**, *112*, 1825.
(2) Goldsmith, S.; Cetinorgu, E.; Boxman, R. L. *Thin Solid Films* **2009**, *517*, 5146.
(3) Diéguez, A.; Romano-Rodríguez, A.; Morante, J. R.; Weimar, U.; Schweizer-Berberich, M.; Göpel, W. *Sens. Actuators, B* **1996**, *31*, 1.
(4) Punnoose, A.; Hays, J.; Thurber, A.; Engelhard, M. H.; Kukkadapu, R. K.; Wang, C.; Shutthanandan, V.; Thevuthasan, S. *Phys. Rev. B* **2005**, *72*, 054402.
(5) Kimura, H.; Fukumura, T.; Kawasaki, M.; Inaba, K.; Hasegawa, T.; Koinuma, H. *Appl. Phys. Lett.* **2002**, *80*, 94.
(6) Xiao, Y. H.; Ge, S. H.; Xi, L.; Zuo, Y. L.; Zhou, X. Y.; Zhang, B. M.; Zhang, L.; Li, C. X.; Han, X. F.; Wen, Z. C. *Appl. Surf. Sci.* **2008**, *254*, 7459.
(7) Hirata, T.; Ishioka, K.; Kitajima, M.; Doi, H. *Phys. Rev. B* **1996**, *53*, 8442.
(8) Ghosh, C. K.; Malkhand, S.; Mitra, M. K.; Chattopadhyay, K. K. *J. Phys. D: Appl. Phys.* **2008**, *41*, 245113.
(9) Mathew, X.; Enriquez, J. P.; Mejia-Garcia, C.; Contreras-Puente, G.; Cortes-Jacome, M. A.; Toledo-Antonio, J. A.; Hays, J.; Punnoose, A. *J. Appl. Phys.* **2006**, *100*, 073907.
(10) Srinivas, K.; Vithal, M.; Sreedhar, B.; Raja, M. M.; Reddy, P. V. *J. Phys. Chem. C* **2009**, *113*, 3543.
(11) Luo, S. H.; Chu, P. K.; Liu, W. L.; Zhang, M.; Lin, C. L. *Appl. Phys. Lett.* **2006**, *88*, 183112.
(12) Hu, J. Q.; Bando, Y.; Liu, Q. L.; Golberg, D. *Adv. Funct. Mater.* **2003**, *13*, 493.
(13) Zhou, X. T.; Heigl, F.; Murphy, M. W.; Sham, T. K.; Regier, T.; Coulthard, I.; Blyth, R. I. R. *Appl. Phys. Lett.* **2006**, *89*, 213109.
(14) Jeong, J.; Choi, S. P.; Chang, C. I.; Shin, D. C.; Park, J. S.; Lee, B. T.; Park, Y. J.; Song, H. J. *Solid State Commun.* **2003**, *127*, 595.
(15) Yuan, Z. Z.; Li, D. S.; Wang, M. H.; Chen, P. L.; Gong, D. R.; Cheng, P. H.; Yang, D. R. *Appl. Phys. Lett.* **2008**, *92*, 121908.
(16) Rani, S. J.; Roy, S. C.; Karar, N.; Bhatnagar, M. C. *Solid State Commun.* **2007**, *141*, 214.
(17) Hu, Z. G.; Li, W. W.; Wu, J. D.; Sun, J.; Shu, Q. W.; Zhong, X. X.; Zhu, Z. Q.; Chu, J. H. *Appl. Phys. Lett.* **2008**, *93*, 181910.
(18) Gao, K.; Zhang, W.; Sun, J.; Xu, N.; Ying, Z. F.; Li, Q.; Gan, J.; Wu, J. D. *J. Phys. Chem. C* **2009**, *113*, 19139.
(19) Komen, C. V.; Thurber, A.; Reddy, K. M.; Hays, J.; Punnoose, A. *J. Appl. Phys.* **2008**, *103*, 07D141.
(20) Gopinadhan, K.; Kashyap, S. C.; Pandya, D. K.; Chaudhary, S. *J. Appl. Phys.* **2007**, *102*, 113513.
(21) Hays, J.; Punnoose, A.; Baldner, R.; Engelhard, M. H.; Peloquin, J.; Reddy, K. M. *Phys. Rev. B* **2005**, *72*, 075203.

(22) Hu, Z. G.; Rinzan, M. B. M.; Matsik, S. G.; Perera, A. G. U.; Winckel, G. V.; Stintz, A.; Krishna, S. *J. Appl. Phys.* **2005**, *97*, 093529.

(23) Heaven, O. S. *Optical Properties of Thin Solid Films*; Dover: NewYork, 1991; Chapter 4, p 69.

(24) Kim, T. W.; Lee, D. U.; Choo, D. C.; Kim, J. H.; Kim, H. J.; Jeong, J. H.; Jung, M.; Bahang, J. H.; Park, H. L.; Yoon, Y. S.; Kim, J. Y. *J. Phys. Chem. Solids* **2002**, *63*, 881.

(25) Li, W. W.; Hu, Z. G.; Wu, J. D.; Sun, J.; Zhu, M.; Zhu, Z. Q.; Chu, J. H. *J. Phys. Chem. C* **2009**, *113*, 18347.

(26) Djurišić, A. B.; Chan, Y.; Li, E. H. *Mater. Sci. Eng., R* **2002**, *38*, 237.

(27) Herzinger, C. M.; Johs, B.; McGahan, W. A.; Woollam, J. A.; Paulson, W. *J. Appl. Phys.* **1998**, *83*, 3323.

(28) Ogale, S. B.; Choudhary, R. J.; Buban, J. P.; Lofland, S. E.; Shinde, S. R.; Kale, S. N.; Kulkarni, V. N.; Higgins, J.; Lanci, C.; Simpson, J. R.; Browning, N. D.; Das Sarma, S.; Drew, H. D.; Greene, R. L.; Venkatesan, T. *Phys. Rev. Lett.* **2003**, *91*, 077205.

(29) Mishra, K. C.; Johnson, K. H.; Schmidt, P. C. *Phys. Rev. B* **1995**, *51*, 13972.

(30) Wang, X. L.; Dai, Z. X.; Zeng, Z. *J. Phys.: Condens. Matter* **2008**, *20*, 045214.

(31) Park, Y. R.; Kim, K. J. *J. Appl. Phys.* **2003**, *94*, 6401.

(32) Singh, S.; Ramachandra Rao, M. S. *Phys. Rev. B* **2009**, *80*, 045210.

(33) Samanta, K.; Dussan, S.; Katiyar, R. S.; Bhattacharya, P. *Appl. Phys. Lett.* **2007**, *90*, 261903.

(34) Katiyar, R. S.; Dawson, P.; Hargreave, M. M.; Wilkinson, G. R. *J. Phys. C: Solid State Phys.* **1971**, *4*, 2421.

(35) Hu, Z. G.; Weerasekara, A. B.; Dietz, N.; Perera, A. G. U.; Strassburg, M.; Kane, M. H.; Asghar, A.; Ferguson, I. T. *Phys. Rev. B* **2007**, *75*, 205320.

(36) Zhang, H.; Liu, Y. L.; Zhu, K.; Siu, G. G.; Xiong, Y. H.; Xiong, C. S. *J. Phys.: Condens. Matter* **1998**, *10*, 11121.

(37) Yu, B. L.; Guo, L. J.; Yang, Z. T.; Zhu, C. S.; Gan, F. X.; Zhang, G. L.; Tang, G. Q.; Wu, X. C.; Chen, W. J. *Phys. Lett. A* **1999**, *251*, 67.

(38) Kim, H. S.; Bi, L.; Dionne, G. F.; Ross, C. A. *Phys. Rev. B* **2008**, *77*, 214436.

(39) Kim, K. J.; Park, Y. R. *Appl. Phys. Lett.* **2002**, *81*, 1420.

(40) Xiang, X.; Zu, X. T.; Wan, L. M.; Shutthanadan, V.; Nachimuthu, P.; Zhang, Y. *J. Phys. D: Appl. Phys.* **2008**, *41*, 225102.

(41) Brivekku, S.; Chiodini, N.; Meinardi, F.; Lauria, A.; Paleari, A. *Appl. Phys. Lett.* **2006**, *89*, 153126.

(42) Hu, J. Q.; Ma, X. L.; Shang, N. G.; Xie, Z. Y.; Wong, N. B.; Lee, C. S.; Lee, S. T. *J. Phys. Chem. B* **2002**, *106*, 3823.

(43) Wu, J.; Yu, K.; Li, L. J.; Xu, J. W.; Shang, D. J.; Xu, Y.; Zhu, Z. Q. *J. Phys. D: Appl. Phys.* **2008**, *41*, 185302.

(44) Zhou, W. C.; Liu, R. B.; Wan, Q.; Zhang, Q. L.; Pan, A. L.; Guo, L.; Zou, B. S. *J. Phys. Chem. C* **2009**, *113*, 1719.

(45) Chen, H. T.; Wu, X. L.; Xiong, S. J.; Zhang, W. C.; Zhu, J. *Appl. Phys. A* **2009**, *97*, 365.

(46) Luttinger, J. M.; Kohn, W. *Phys. Rev.* **1955**, *97*, 869.

JP101344D